THE ASTROPHYSICAL JOURNAL, 341:847–856, 1989 June 15

THE SPATIAL DISTRIBUTION OF THE OH MASERS IN ORION-KL

K. J. JOHNSTON
E. O. Hulburt Center for Space Research, Naval Research Laboratory

V. MIGENES
Astronomy Department, University of Pennsylvania

AND

R. P. NORRIS
C.S.I.R.O., Epping, New South Wales
Received 1986 November 17; accepted 1988 September 29

ABSTRACT

The OH maser emission associated with Orion-KL in the velocity range -5 through 25 km s^{-1} LSR has been mapped to a level of 0.5 Jy in the 1665 MHz and 1612 MHz OH transitions. The majority of the masers have been found to have an east-west distribution of length of 14″ encompassing the sources IRc2, IRc7, and IRc6. These masers are located along a ridge defined by the NH_3 emission associated with dense, hot regions. Other areas of OH emission with velocities near 18 km s^{-1} are found 5″–10″ from this emission. The OH masers appear to be in "clumps" with dispersions of 2–6 km s^{-1} and are probably formed in turbulent regions near the edges of shock fronts. The distribution of the maser emission is quite complex and is consistent with models describing a "cavity" or an outflow caused by one or more exciting sources.

Subject headings: interstellar: molecules — masers — nebulae: Orion Nebula

I. INTRODUCTION

The Orion Molecular Cloud (OMC-1) is one of the closest and most intensely studied regions in the Galaxy. The maser emission associated with Orion-KL in OMC-1 arising from the OH, H_2O, and SiO molecules has been extensively studied (Menon 1967; Palmer and Zuckerman 1967; Knowles *et al.* 1969; Sullivan 1973; Buhl *et al.* 1974). Interferometry has allowed the spatial distribution of the OH and H_2O maser emission on scales of arc seconds to be measured (Hansen and Johnston 1983). This emission has been found to be divided into two populations: a low-velocity flow, spatially distributed in such a configuration which can be ascribed to mass loss from IRc2; while the other, a high-velocity flow, is due to an isotropic outflow probably from the same source (Genzel *et al.* 1981; Norris 1984). Measurement of the radial velocity and proper motion of the high-velocity H_2O masers appear to indicate an expansion from IRc2, allowing the distance to IRc2 to be determined to be 480 ± 80 pc (Genzel *et al.* 1981).

New observations with the VLA have allowed us to map the OH masers with greater sensitivity than the previous measurements by Hansen and Johnston (1983). With these new measurements we were able to detect emission as low as 0.5 Jy and map multiple features in each spectral channel, in contrast to the previous VLA measurements which were made when the spectral line system was in its infancy. In those earlier measurements six antennas were used over a 4 hr period and only the peak feature in each spectral channel was mapped, so that a total of 80 maser features were measured. Here we report the location of 166 features. The association of these features with an outflow from IRc2 is discussed.

II. OBSERVATIONS AND RESULTS

The VLA was used on 1985 January 7 from 0 to 12 hours IAT to map the 1612 and 1665 MHz OH emission in right-hand and left-hand circular polarization. We used 13 antennas in the "A" configuration. Scans of 10 minute duration at both frequencies and polarizations were obtained every hour interspersed with observations of the calibrator 0500+019. The flux density scale was established by assuming that 3C 48 was 14.23 and 13.85 Jy at 1612 and 1665 MHz, respectively. The total bandwidth of the observations was 390.625 kHz. Onehundred and twenty-eight channels with on-line Hanning weighting were employed using the inner 195.3 kHz, giving a channel separation of 1.5 kHz (0.3 km s^{-1}). The source 0500+019 was used to calibrate the instrumental amplitude and phases. No taper was applied to the *u-v* data in order to obtain the highest angular resolution. The individual spectral channels were mapped using a cell size of 0.″3 and an image size of 512 × 512 pixels. This cell size was chosen since the synthesized beam was 1.″2 × 1.″0 for all the transitions with a p.a. of $-12°$ for the 1665 MHz and a similar beam size with a p.a. 6° for the 1612 MHz transition. The inner quarter of these maps was cleaned. The data were then self-calibrated using a strong feature in each spectrum. The spectral channels were again mapped, and the relative positions of the spectral features were found.

The radial velocities with respect to the local standard of rest (LSR) were calculated by using 1665.401 MHz and 1612.231 MHz as the rest frequencies for the OH transitions. The observed band of 35 km s^{-1} width was centered on 7.5 km s^{-1}. The majority of the channels displayed maser features which were observed in several spectral channels. The velocity at peak emission was chosen as the velocity of the feature. The positions of the various features in one channel were compared; if the difference in position, over several spectral channels, was larger than the accuracy of our measurements, then it was assumed to be due to a superposition of features. The positions were determined by fitting a two-dimensional Gaussian brightness distribution to each component.

The maser feature with a velocity of 9.1 km s^{-1} did not appear to change its position since observations taken in 1980 by Hansen and Johnston (1983), and thus it was chosen as the reference position for the 1665 RCP and LCP masers. The

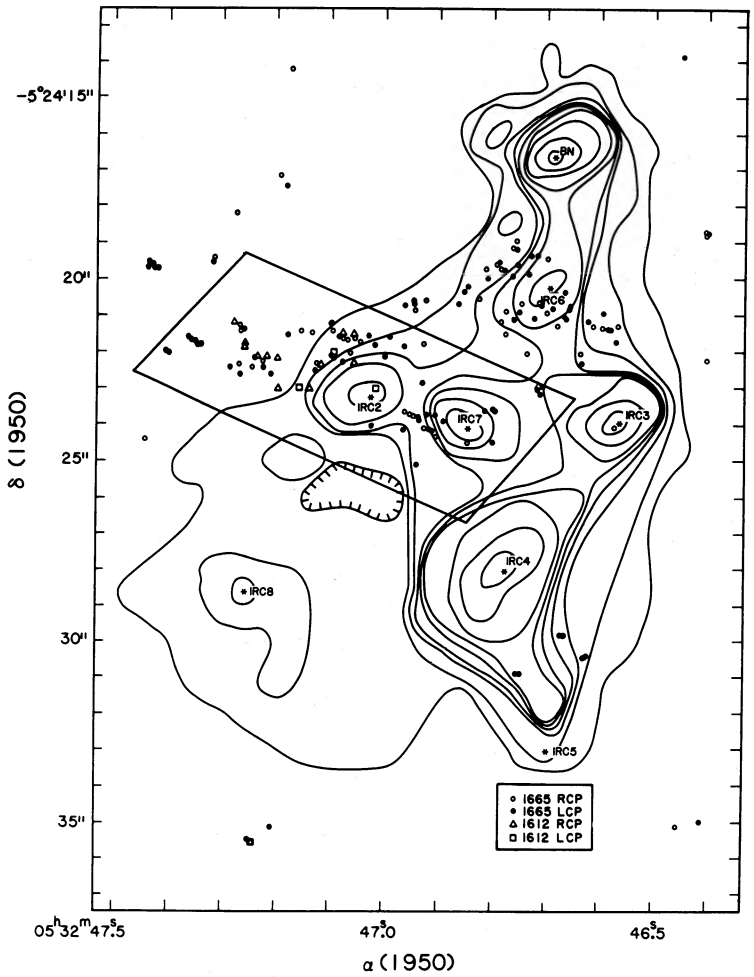

FIG. 1.—Distribution of the OH masers in the velocity range −5 to 25 km s^{-1} near Orion-KL. The contours denote the 20 μm emission. The solid lines forming the rectangle around IRc2 are where the majority of the earlier OH masers were found.

reference features for the 1612 RCP and LCP data were those at 8.6 km s^{-1} and 8.1 km s^{-1}, respectively. The positions of these reference features were used to place the masers on the map shown in Figure 1. Their absolute positions along with the position of the calibrator 0500+019 are listed in Table 1. The errors in the absolute position of the reference features is the formal error of the measurements. Although positions can be routinely determined with the VLA to a hundredth of an arcsecond (Johnston *et al.* 1985), the uncertainty in the absolute position of these features is 0".05 due to our lack of knowledge of the position of the calibrator 0500+019. The formal errors are listed in Table 1 for the reference feature so that the error in the positions may be reduced when an improved position is available for 0500+019. The relative positions with respect to the reference features are listed in Table 2. The accuracy of the relative positions is limited by the strength of the spectral feature, and systematic errors in the Gaussian fit routine. The accuracy of the relative positions of strong features is 3 mas.

III. DISCUSSION

Before discussing the spatial distribution of the OH maser emission, let us review the 1612 and 1665 MHz spectra. Figure 2 displays 1665 OH spectra obtained between 1965 and 1986.

TABLE 1

POSITIONS FOR THE REFERENCE MASER FEATURES AND THE CALIBRATOR EPOCH OF OBSERVATIONS 1985.017

Feature	R.A. (1950)	Decl. (1950)	Flux (Jy)
0500+019	$05^h00^m45^s.183 \pm 0^s.050$	$+01°58'53".82 \pm 0".005$	2.39
9.1 km s^{-1} (1665 RCP)	05 32 46.8066 ± 0.005	−05 24 24.501 ± 0.006	3.10
9.1 km s^{-1} (1665 LCP)	05 32 46.8028 ± 0.005	−05 24 24.488 ± 0.005	26.70
8.1 km s^{-1} (1612 RCP)	05 32 46.8001 ± 0.005	−05 24 24.491 ± 0.003	7.80
8.6 km s^{-1} (1612 LCP)	05 32 46.7998 ± 0.006	−05 24 24.498 ± 0.003	4.30

TABLE 2

RELATIVE POSITIONS OF THE OH MASERS IN THE OMC-1

Transition	Radial Velocity (LSR) (km s^{-1})	$\Delta\alpha \cos\delta$	$\Delta\delta$	Flux (Jy)	FWHM (km s^{-1})
1665 RCP.....	23.7	−0.″039 ± 0.″010	4.″901 ± 0.″006	0.5	0.6
	23.7	7.743 ± 0.006	5.057 ± 0.003	3.2	0.7
	23.4	4.180 ± 0.010	2.878 ± 0.006	0.4	0.5
	23.1	6.996 ± 0.006	3.200 ± 0.003	5.0	1.1
	22.6	−0.614 ± 0.010	5.565 ± 0.003	1.0	0.6
	22.3	5.327 ± 0.003	3.044 ± 0.003	6.0	1.0
	21.7	−0.510 ± 0.010	5.365 ± 0.030	1.0	0.2
	21.2	6.710 ± 0.003	2.378 ± 0.003	11.3	0.5
	20.9	6.393 ± 0.003	2.204 ± 0.003	10.4	0.4
	20.7	0.237 ± 0.006	4.770 ± 0.003	1.4	1.0
	20.7	1.952 ± 0.010	2.681 ± 0.009	0.4	0.3
	20.1	9.678 ± 0.010	0.025 ± 0.015	0.5	0.3
	20.1	7.062 ± 0.003	2.141 ± 0.003	18.8	0.5
	19.8	−1.493 ± 0.006	5.030 ± 0.006	0.9	1.0
	19.3	7.292 ± 0.006	2.044 ± 0.006	0.9	0.6
	18.7	4.938 ± 0.003	2.147 ± 0.003	18.6	0.9
	16.8	−0.678 ± 0.006	4.812 ± 0.003	0.6	1.1
	16.0	4.523 ± 0.010	2.295 ± 0.003	1.4	1.1
	16.0	8.570 ± 0.010	2.885 ± 0.003	3.2	1.1
	15.4	−0.201 ± 0.015	4.776 ± 0.003	0.9	0.4
	14.9	−0.471 ± 0.010	4.583 ± 0.003	2.2	0.7
	14.1	8.367 ± 0.010	2.822 ± 0.003	1.2	1.0
	14.1	3.990 ± 0.010	2.444 ± 0.003	1.4	0.8
	13.2	7.217 ± 0.015	6.344 ± 0.003	1.1	0.6
	12.7	3.824 ± 0.010	2.735 ± 0.003	0.8	0.5
	12.1	9.054 ± 0.009	2.504 ± 0.003	1.8	0.4
	11.3	3.974 ± 0.006	2.822 ± 0.003	6.9	1.5
	11.0	−0.672 ± 0.010	−6.460 ± 0.003	1.2	0.9
	10.8	8.241 ± 0.010	2.755 ± 0.003	1.7	0.6
	9.4	−2.633 ± 0.020	−6.085 ± 0.009	0.6	0.3
	9.1	3.837 ± 0.010	2.841 ± 0.003	1.1	0.9
	9.1	0.069 ± 0.020	0.009 ± 0.003	3.0	0.8
	9.1	9.605 ± 0.009	4.782 ± 0.003	1.4	0.6
	9.1	5.052 ± 0.009	3.011 ± 0.003	0.7	0.3
	8.6	9.392 ± 0.009	4.793 ± 0.003	1.0	0.4
	8.3	−2.022 ± 0.009	−5.437 ± 0.003	1.0	0.8
	7.7	−5.118 ± 0.006	−10.627 ± 0.003	4.7	0.3
	7.7	1.463 ± 0.006	0.122 ± 0.003	1.9	0.4
	7.5	−2.157 ± 0.006	−0.013 ± 0.003	5.8	0.3
	7.2	6.707 ± 0.006	−11.009 ± 0.003	1.3	0.3
	7.2	−2.145 ± 0.006	3.623 ± 0.003	1.3	0.5
	6.9	9.587 ± 0.015	4.945 ± 0.006	0.8	0.3
	6.7	−1.364 ± 0.003	3.776 ± 0.003	3.0	0.6
	6.1	0.239 ± 0.015	0.851 ± 0.006	0.7	1.1
	6.1	−5.702 ± 0.015	5.893 ± 0.006	3.3	0.3
	5.8	5.724 ± 0.006	−10.231 ± 0.003	1.5	0.6
	5.8	2.202 ± 0.009	3.871 ± 0.003	1.1	0.7
	5.8	−0.764 ± 0.009	3.814 ± 0.003	1.3	0.9
	5.6	−5.909 ± 0.006	5.755 ± 0.006	1.2	0.8
	5.3	1.885 ± 0.006	0.368 ± 0.003	1.8	0.5
	5.0	−3.498 ± 0.020	3.236 ± 0.009	0.4	0.4
	4.2	−2.960 ± 0.006	3.153 ± 0.006	2.0	0.7
	3.9	0.035 ± 0.003	0.884 ± 0.003	22.5	0.8
	3.9	−1.263 ± 0.006	3.651 ± 0.003	1.3	0.9
	2.8	−2.147 ± 0.006	3.534 ± 0.003	0.5	...
	2.5	2.211 ± 0.006	0.725 ± 0.003	3.2	1.0
	2.5	5.712 ± 0.006	4.084 ± 0.003	1.3	...
	2.3	−0.063 ± 0.009	0.871 ± 0.006	1.6	0.9
	1.7	−1.497 ± 0.015	3.560 ± 0.012	0.7	0.3
	0.9	4.455 ± 0.003	3.197 ± 0.006	3.7	0.5
	0.9	−5.897 ± 0.003	2.538 ± 0.006	0.6	0.6
	0.6	−5.913 ± 0.010	2.281 ± 0.006	0.8	0.3
	0.3	2.441 ± 0.010	0.845 ± 0.009	0.7	0.7
	0.3	4.446 ± 0.009	3.066 ± 0.006	1.2	0.5
	0.1	−2.702 ± 0.009	3.203 ± 0.006	1.0	1.0
	−0.7	2.373 ± 0.006	0.752 ± 0.003	3.0	0.6
	−1.3	−3.222 ± 0.015	3.244 ± 0.009	0.9	1.3
	−1.3	0.339 ± 0.003	3.989 ± 0.006	1.3	0.4
	−1.5	5.945 ± 0.020	7.330 ± 0.012	0.9	0.3
	−1.8	−3.222 ± 0.020	3.140 ± 0.012	0.5	1.1

TABLE 2—*Continued*

Transition	Radial Velocity (LSR) (km s^{-1})	$\Delta\alpha \cos\delta$	$\Delta\delta$	Flux (Jy)	FWHM (km s^{-1})
	−2.9	−1.301 ± 0.009	1.406 ± 0.009	0.9	0.4
	−2.9	−0.352 ± 0.009	3.595 ± 0.009	0.8	0.6
	−4.0	3.365 ± 0.003	0.422 ± 0.000	5.0	0.6
	−4.8	1.590 ± 0.006	0.746 ± 0.006	1.5	0.5
	−5.4	−2.016 ± 0.006	2.459 ± 0.006	2.0	1.1
	−5.4	2.174 ± 0.006	3.611 ± 0.006	1.1	0.3
	−5.7	0.213 ± 0.003	3.372 ± 0.006	1.7	0.5
	−6.7	0.731 ± 0.003	−0.022 ± 0.003	1.3	0.7
	−6.7	1.878 ± 0.010	3.899 ± 0.006	0.8	1.0
	−7.0	−2.455 ± 0.020	2.242 ± 0.006	0.7	0.4
	−8.1	−0.339 ± 0.025	2.991 ± 0.006	0.5	1.0
1665 LCP.....	24.2	2.453 ± 0.005	2.635 ± 0.015	0.6	0.2
	24.2	4.241 ± 0.005	2.865 ± 0.003	0.6	0.2
	23.9	7.761 ± 0.005	4.955 ± 0.003	1.2	0.7
	23.7	0.168 ± 0.005	4.506 ± 0.006	0.3	0.5
	23.1	3.420 ± 0.009	2.860 ± 0.006	0.3	0.6
	22.8	6.932 ± 0.010	3.117 ± 0.006	3.8	1.1
	22.8	−0.626 ± 0.005	5.285 ± 0.006	1.2	1.1
	22.3	5.711 ± 0.006	2.951 ± 0.003	3.7	0.8
	21.2	6.356 ± 0.003	2.045 ± 0.006	6.1	1.4
	20.9	−0.296 ± 0.009	4.723 ± 0.009	0.4	1.1
	19.6	7.010 ± 0.005	1.822 ± 0.003	2.6	1.0
	19.3	−1.064 ± 0.005	5.125 ± 0.006	0.5	1.0
	18.7	4.967 ± 0.003	1.939 ± 0.003	6.8	1.0
	18.5	0.806 ± 0.003	4.167 ± 0.003	0.4	0.5
	17.9	4.506 ± 0.005	2.383 ± 0.003	4.7	0.9
	17.3	−0.131 ± 0.012	4.934 ± 0.015	0.4	0.2
	16.3	4.170 ± 0.005	2.203 ± 0.006	1.6	0.9
	16.0	−0.960 ± 0.005	4.628 ± 0.003	0.9	0.9
	16.0	3.002 ± 0.005	2.392 ± 0.006	1.6	1.1
	16.0	8.451 ± 0.005	2.816 ± 0.003	6.8	1.0
	14.6	2.505 ± 0.009	0.313 ± 0.006	0.8	0.6
	14.1	8.268 ± 0.005	2.813 ± 0.003	1.8	0.9
	13.5	0.717 ± 0.005	4.304 ± 0.003	0.5	0.3
	13.2	3.272 ± 0.005	2.671 ± 0.003	0.5	0.4
	13.0	2.015 ± 0.005	0.596 ± 0.003	2.6	0.8
	13.0	−1.977 ± 0.005	4.111 ± 0.003	0.4	0.2
	12.7	1.832 ± 0.005	0.701 ± 0.009	1.8	0.8
	12.1	9.003 ± 0.005	2.474 ± 0.003	0.8	0.4
	12.1	2.886 ± 0.005	2.888 ± 0.009	2.2	0.4
	11.3	1.698 ± 0.005	0.284 ± 0.003	2.6	1.1
	10.8	−0.809 ± 0.005	−6.430 ± 0.009	0.9	0.9
	10.8	8.138 ± 0.005	2.747 ± 0.003	1.7	0.6
	10.2	−3.084 ± 0.005	3.560 ± 0.003	0.7	0.5
	9.7	1.746 ± 0.005	0.299 ± 0.003	3.5	0.5
	9.7	−2.651 ± 0.005	−5.958 ± 0.003	0.6	0.3
	9.4	2.208 ± 0.005	3.715 ± 0.003	0.8	0.3
	9.1	−0.011 ± 0.005	0.070 ± 0.003	26.7	1.5
	8.6	9.320 ± 0.005	4.724 ± 0.003	1.6	0.9
	8.6	−1.916 ± 0.005	−5.339 ± 0.003	0.4	0.5
	8.0	−2.157 ± 0.005	3.749 ± 0.003	0.7	0.9
	7.7	6.056 ± 0.005	−10.669 ± 0.003	2.6	0.7
	7.7	−5.220 ± 0.005	−10.669 ± 0.003	2.9	0.3
	7.5	5.858 ± 0.005	−10.504 ± 0.003	2.3	0.6
	7.2	3.467 ± 0.005	−13.060 ± 0.003	0.5	0.6
	7.2	9.471 ± 0.005	4.875 ± 0.003	0.6	0.3
	6.4	−5.913 ± 0.005	5.771 ± 0.003	2.1	1.6
	6.1	−2.666 ± 0.010	3.314 ± 0.003	0.7	0.8
	5.8	2.195 ± 0.015	3.842 ± 0.006	0.7	0.2
	4.5	2.049 ± 0.005	0.612 ± 0.006	2.2	1.3
	4.5	−1.137 ± 0.005	3.421 ± 0.006	1.1	0.4
	4.2	−3.236 ± 0.005	3.125 ± 0.003	1.3	0.6
	3.9	−2.013 ± 0.005	3.421 ± 0.003	0.9	0.3
	3.4	−0.732 ± 0.005	3.602 ± 0.003	0.6	0.3
	3.1	1.982 ± 0.005	1.640 ± 0.003	1.4	0.4
	2.5	2.108 ± 0.005	−0.671 ± 0.003	1.0	0.3
	1.7	−1.661 ± 0.005	3.672 ± 0.003	1.4	0.3
	−2.6	−3.429 ± 0.025	2.750 ± 0.015	0.4	0.2
	−2.6	−1.347 ± 0.010	1.365 ± 0.006	0.8	0.4
	−3.2	5.741 ± 0.010	7.032 ± 0.006	0.7	0.6
	−4.8	1.415 ± 0.008	0.679 ± 0.003	2.6	0.7

TABLE 2—*Continued*

Transition	Radial Velocity (LSR) (km s^{-1})	$\Delta\alpha \cos\delta$	$\Delta\delta$	Flux (Jy)	FWHM (km s^{-1})
	−5.4	−0.423 ± 0.005	3.407 ± 0.009	1.2	1.3
	−6.5	0.966 ± 0.005	3.800 ± 0.003	2.0	0.7
	−7.0	−2.472 ± 0.008	2.184 ± 0.009	0.4	0.3
1612 RCP.....	22.8	6.890 ± 0.020	2.611 ± 0.009	0.3	0.3
	22.5	7.187 ± 0.020	3.209 ± 0.010	0.3	0.3
	21.8	6.888 ± 0.020	2.695 ± 0.009	0.3	0.5
	21.1	6.567 ± 0.015	2.395 ± 0.006	0.9	0.6
	20.2	5.987 ± 0.020	1.490 ± 0.006	0.5	0.3
	19.1	5.091 ± 0.015	1.490 ± 0.006	1.1	1.1
	17.1	5.993 ± 0.015	2.485 ± 0.006	0.9	0.6
	16.6	6.288 ± 0.015	2.389 ± 0.006	1.1	0.5
	16.0	4.793 ± 0.015	2.097 ± 0.006	0.3	0.3
	14.6	4.472 ± 0.010	2.390 ± 0.006	1.4	0.8
	12.3	3.878 ± 0.015	2.696 ± 0.006	0.8	1.3
	11.2	4.172 ± 0.020	3.004 ± 0.020	0.3	0.4
	8.6	3.854 ± 0.015	2.991 ± 0.020	0.6	0.3
	8.1	−0.029 ± 0.005	0.002 ± 0.003	7.7	0.5
	7.5	6.590 ± 0.010	−11.112 ± 0.006	1.4	0.3
	−2.4	−1.244 ± 0.020	1.491 ± 0.020	0.5	0.8
1612 LCP.....	20.8	3.272 ± 0.020	9.890 ± 0.015	0.3	0.3
	19.4	5.093 ± 0.020	1.188 ± 0.020	0.4	0.5
	14.9	4.476 ± 0.020	2.392 ± 0.020	0.3	0.5
	8.6	−0.035 ± 0.010	0.005 ± 0.006	1.3	0.3
	7.8	6.589 ± 0.020	−11.109 ± 0.020	0.3	0.3

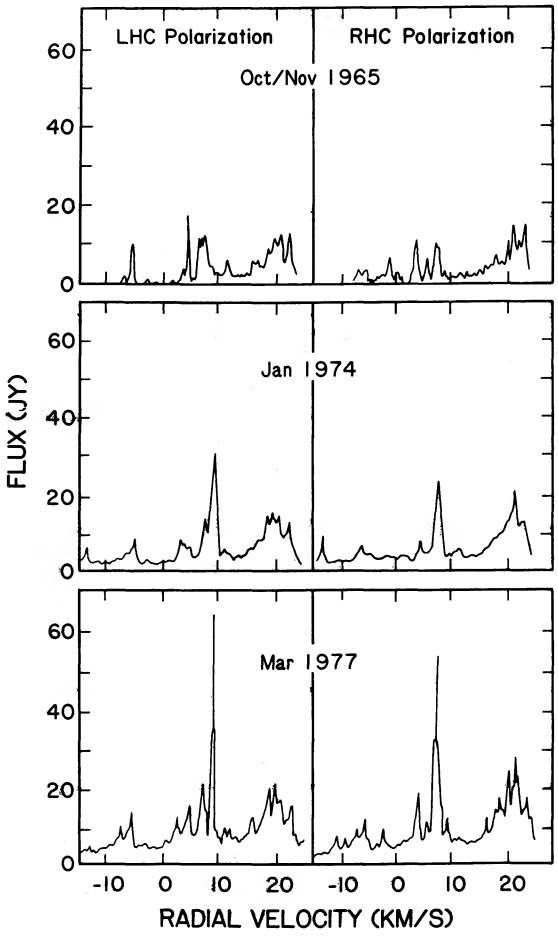

FIG. 2*a*

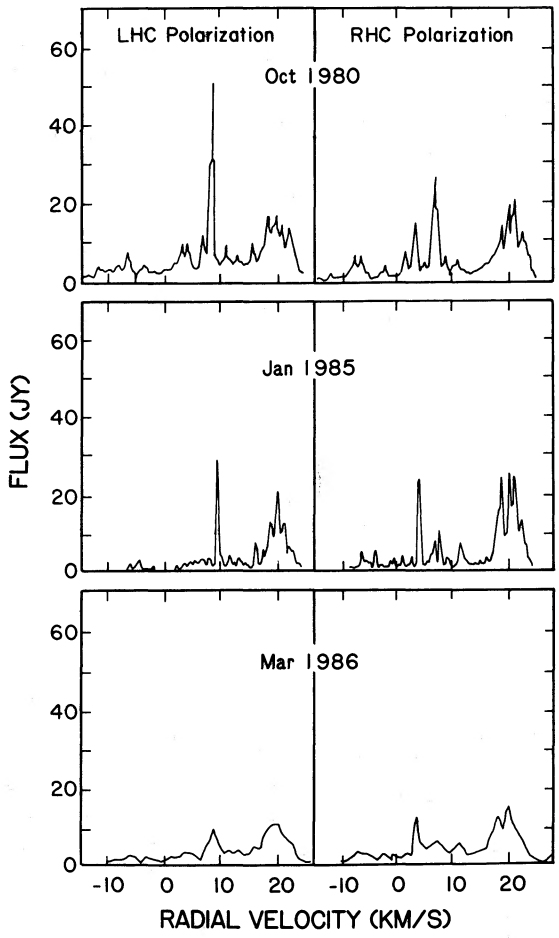

FIG. 2*b*

FIG. 2.—Spectra at 1665 MHz of Orion-KL for the time period 1965 through 1986. Comparison of these spectra is difficult as they have been obtained with different spatial and spectral resolutions. However, variations are evident at radial velocities of 20 km s^{-1} and 4 km s^{-1}. The regularly spaced vertical spikes in the velocity axes are tick marks.

These spectra were obtained with different spectral resolutions, telescopes, and techniques. The 1965 spectra were obtained with the 140 foot (42.6 m) telescope (field of view 18′) with a velocity resolution of 0.25 km/s (Palmer and Zuckerman 1967). The Jan 74, Mar 77 and Oct 80 spectra have velocity resolutions of 0.6, 0.1, and 0.3 km s^{-1}, respectively (Norris 1984). The 1980 September spectra were obtained with the 140 foot telescope with a spectral resolution of 0.1 km s^{-1} (Johnston and Hansen 1983). The 1985 January spectra are from the observation reported here and are the sum of all spectral features within 19″ of IRc2 with a velocity resolution of 0.3 km s^{-1}. The spectra of 1986 March were again obtained with the 140 foot telescope with a velocity resolution of 0.9 km s^{-1} (Madalena 1986).

Comparison of these spectra must be made with caution because of their lack of uniformity in spectral and spatial resolution. The intensity of the group of features near 20 km s^{-1} is approximately 20 Jy at all epochs. However, the detailed shape of the spectra near this radial velocity appears to change with time. The strong feature near 4 km s^{-1} seen in the 1965 spectra is much weaker in the later spectra, and the strong feature near 8 km s^{-1} reached a peak of over 100 Jy in 1978 (R. P. Norris, unpublished data) but has since weakened. The 1612 OH spectra (Fig. 3) were obtained with the 140 foot telescope with a velocity resolution of 0.1 km s^{-1} in 1980, and with the VLA with a velocity resolution of 0.3 km s^{-1} for the 1985 spectra. No significant change is seen in the RCP spectra, but the LCP spectrum shows a 80% reduction in flux density.

This data set is far from ideal for detailed comparison of spectral features, but it can be said with confidence that the OH spectrum shows considerable variation over the interval 1965–1986. There are probably variations on time scales as short as a year as comparison of the 1985 January and 1986 March spectra crudely show. Therefore, detailed comparison of the spatial distribution of OH emission in Orion-KL obtained at different epochs should be made with care.

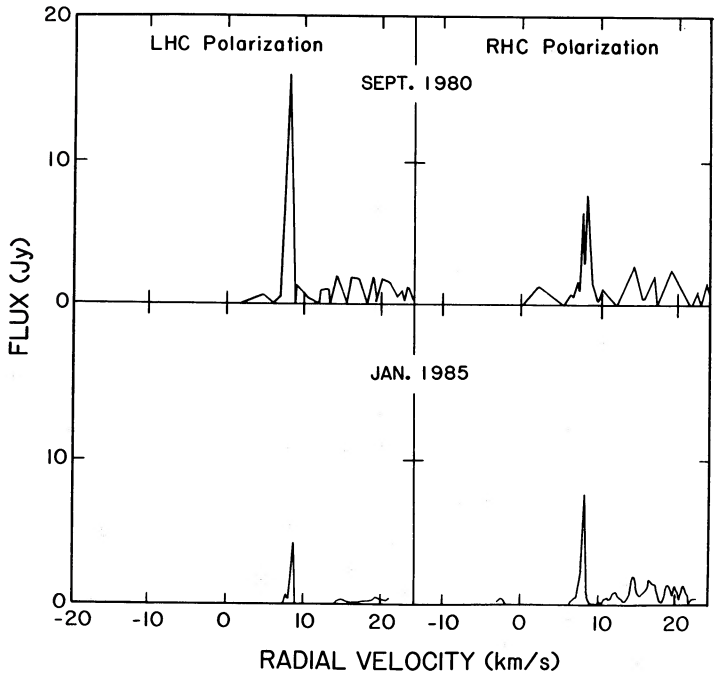

FIG. 3.—Spectra at 1612 MHz of Orion-KL for 1980 and 1985 epochs

The general spatial distribution of masers agrees well with earlier measurements. Those masers around and to the NE of IRc2 were mapped by Hansen and Johnston (1983) and Norris (1984). The map in Figure 1 also contains many OH maser features not observed before. Most of the new OH features appear NW of IRc2 and fall within a 2″.5 radius of IRc6. A few are less than an arcsecond from IRc7. There are also many centers of maser activity at velocities between 6 and 10 km s^{-1} located at distances up to 10″ from IRc2. There also appears to be a concentration of features south of IRc4 near the H_2O maser features.

Detailed comparison of maser features mapped at other epochs reveals that only 26 (16%) of the features are coincident with features observed in 1980 by Hansen and Johnston (1983), and 24 (16%) with masers observed in 1981 by Norris (1984). Only (9%) are common to all three sets of observations. The positions of the maser features reported for epoch 1979 (Norris 1984) were not used in this comparison because of their poor positional accuracy. Several features near 8 km s^{-1} were found to be coincident within the measurement errors. At the distance to the Orion nebula, a proper motion of 1 mas yr^{-1} will result from a velocity of 10 km s^{-1} perpendicular to the line of sight. Unfortunately, the accuracy of the 1980 and 1981 measurements (0″.2 and 0″.03 in relative position of Norris 1984 and Hansen and Johnston 1983, respectively) are only adequate to detect a proper motion of 8 mas yr^{-1} given the time base of the observations which span the period 1980 to 1985. Therefore, to measure proper motions of OH masers, accuracies in relative position of better than a milliarcsecond must be achieved and the observations will have to be made over a short period of time (a few years) in order to ensure that the same maser feature is being observed.

Many of the features with velocities near 20 km s^{-1} measured at different epochs were found not to be coincident within the errors. This is attributed to variations in the maser spectra and is probably due to different maser features. Masers form when the velocity along the maser path allows coherent amplification. They may then be destroyed by the turbulence in the medium. This may either be followed by the formation nearby of a different maser or else the feature may move around in a given small area. In the latter case it may pass through a slightly different region inducing changes in the maser which cause it to change in amplitude, frequency, or polarization. This effect has been observed in W3 by Norris and Booth (1981). It is certainly difficult to determine whether masers observed at various epochs are exactly the same or represent real changes in the source structure.

The distribution of OH masers appears to be rather clumpy. Figure 4 displays a small area of Figure 1 with the maser velocities labeled. One can identify a clump (NE4) of maser features at a position ($05^h32^m47^s.4$, $-05°24'22''$) with a velocity $\simeq 14$ km s^{-1} containing nine maser features. We have attempted to group all of the masers into specific clumps. These are listed in Table 3 with the number of masers features in a clump, the offset in position from the reference feature, its average velocity, range of velocities, and diameter of the cluster. Northwest of IRc2 (clump NE6) and northwest of IRc6 (clump NW1), the velocities of the clumps are very mixed. This may be due to the superposition of several clumps.

If the gas motions are represented by the velocity dispersion in a clump and are balanced by gravity, i.e., stable, and the

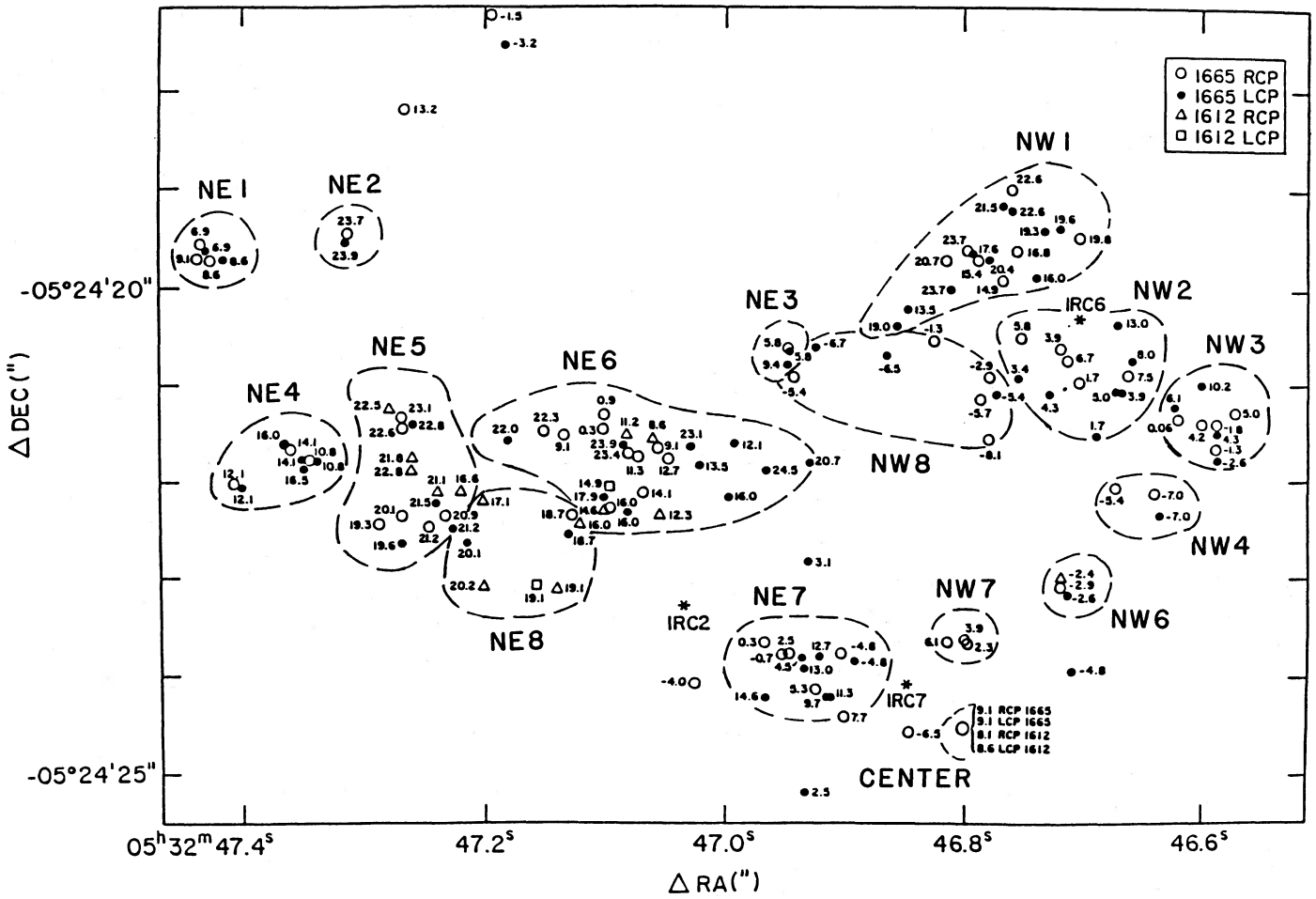

FIG. 4.—Distribution of OH maser emission over smaller area than presented in Fig. 1 with velocity of masers labeled. Note the apparent clumping in velocity of masers denoted by the dotted lines.

TABLE 3

MASER "CLUMPS" IN ORION-KL

"CLUMP"	N	OFFSET		VELOCITY		SIZE	MASS	n(H2)
		R.A.	Decl.	Mean (km s^{-1})	Delta (km s^{-1})		($M_\odot$)	
NE1	5	9".5	4".8	8.0	2.1	0".6	0.8	1.12E+10
NE2	2	7.8	5.0	23.8	0.2	0.1	0.0	3.65E+09
NE3	3	2.3	3.8	7.0	3.6	1.0	3.8	1.18E+10
NE4	9	8.8	2.6	13.6	5.7	1.0	9.5	2.96E+10
NE5	17	6.8	2.4	19.8	6.5	2.0	24.8	9.63E+09
NE6	25	4.0	2.5	15.6	10.5	4.4	142.2	5.19E+09
NE7	13	1.5	0.5	...	17.8	1.2	111.5	2.01E+11
NE8	7	5.4	1.8	19.0	3.0	1.0	2.6	8.21E+09
NW1	19	−0.8	5.0	19.2	9.1	3.0	72.8	8.39E+09
NW2	12	−1.5	3.5	5.4	11.3	1.5	56.2	5.18E+10
NW3	9	−3.2	3.2	...	12.8	1.6	76.9	5.84E+10
NW4	3	−1.8	2.3	−6.5	1.6	0.5	0.4	9.34E+09
NW5	3	−5.9	5.8	6.2	1.1	0.2	0.1	2.76E+10
NW6	3	−1.3	1.4	−2.6	0.5	0.4	0.0	1.43E+09
NW7	3	0.0	0.8	4.1	3.8	0.4	1.7	8.23E+10
NW8	8	0.6	3.5	−5.3	6.8	1.0	13.6	4.22E+10
SW1	6	−1.8	−6.1	9.5	2.7	3.0	6.4	7.39E+08
SW2	2	−5.6	−10.6	7.6	0.2	0.6	0.0	1.01E+08
Center	4	0.0	0.0	8.7	1.0	0.5	0.1	3.65E+09
SE1	4	6.5	−11.0	7.6	0.6	1.0	0.1	3.28E+08

clumps are assumed spherical, virial masses and densities can be calculated. These masses are in the range 0.05–140 $M_\odot$ with hydrogen densities of 10^8–10^{10} cm^{-3}. These values are much too high for both the expected mass of the clumps and for OH maser emission to occur. Therefore, we can assume that these clumps are not stable.

The clumping of maser emission could indicate that masers are found in turbulent regions near the edges of shock fronts. The clumping of maser emission is consistent with a model of a large cavity surrounding IRc2 (Wynn-Williams *et al.* 1984), although this requires other assumptions. Most of the clumps seem to be associated with the "hot core" of ammonia. The distribution of NH_3 "hot core" emission displayed in the (3,3) lines (Pauls *et al.* 1983) is well correlated with the distribution of the OH features. Figure 5 shows the distribution of the (4,4) NH_3 emission (Genzel *et al.* 1982) which is also associated with the "hot core" and "plateau" emission. This is not unexpected as these lines are found in hot, dense clumps of gas. Preliminary results suggest that maser clumps with a given average velocity can be spatially associated with clumps of ammonia with the same velocity. The other IRc sources in the Kleinmann-Low nebula are irregularities in the material around the cavity, and the OH masers would be associated with material on the edges of this cavity where the appropriate densities, temperatures, and velocity distributions, which allow maser amplification, are found. The masers north of the line joining IRc2 and IRc6 would denote the far side of this cavity, while those south would be on the near side. The cavity is very irregular in shape as the masers do not fit a simple spherical distribution.

Alternatively, the clumps of OH emission could be associated with an outflow. The low-velocity H_2O masers have been modeled by Genzel *et al.* (1981) as an expanding spherical outflow with an expanding velocity of 18 km s^{-1} and a radius of 25″. The SiO masers are located within 1″ of IRc2 (Plambeck 1982). The SO emission is located in an 11″ × 19″ region extending along a NW–SE direction and is centered on IRc2 (Plambeck *et al.* 1982). These results are thought to point to IRc2 as the central energy source and the outflow. The H_2 emission is aligned in the NW–SE direction, roughly perpendicular to the molecular distribution.

Figures 1 and 4 suggest a much more complicated picture for any outflow associated with the OH masers in Orion-KL region. The earlier OH map of Hansen and Johnston (1982) displayed the masers within the solid line in Figure 1 and is consistent with the model of Genzel *et al.* (1981). As already stated, these OH masers roughly follow a bipolar distribution: features with velocities > 10 km s^{-1} tend to be located north of a line joining IRc2 and IRc6, while the majority of features with velocities < 10 km s^{-1} tend to be south of this line.

In Figure 6, we have plotted velocities of all the detected OH masers as a function of distance from IRc2. If the masers are consistent with the low-velocity H_2O outflow, they should all lie as they do within the dotted line of Figure 6. This assumes a systemic velocity of 8 km s^{-1}. The clumps were inspected for agreement with the H_2O outflow model. These are shown as the large triangles in Figure 6. Inside the rectangle defined in Figure 1, there is one cluster to the NE with low-velocity and high-velocity features and there is another cluster to the SW with a mixture of components. Outside the rectangle, most of the clusters have velocities near the rest velocity for the Orion-KL.

If the OH masers were located in an outflow described by the low-velocity H_2O masers, we would see the area within the dotted lines in Figure 6 completely populated with points. However, this figure shows that the majority of OH masers are within 8″ and have a velocity range of ± 18 km s^{-1}. Therefore, to be consistent with an outflow described by the H_2O low-velocity masers, the OH masers must be located very near the source of the outflow. This is consistent with the model pro-

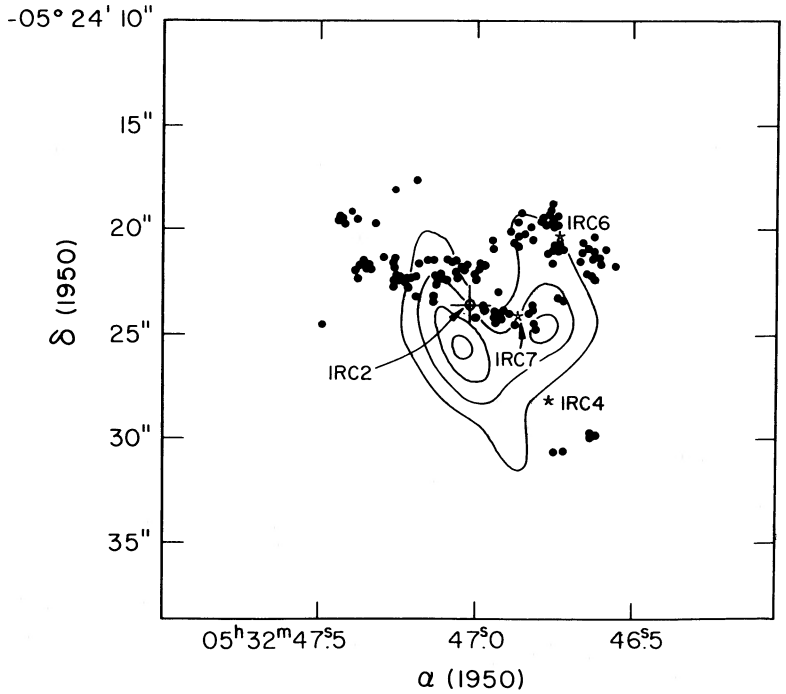

FIG. 5.—The distribution of OH masers (*filled circles*) and contour delineating the hyperfine (4,4) NH_3 line which is associated with the hot core and plateau emission (Genzel *et al.* 1982). This NH_3 emission is associated with dense, hot gas. The various IRc sources are represented by a star symbol.

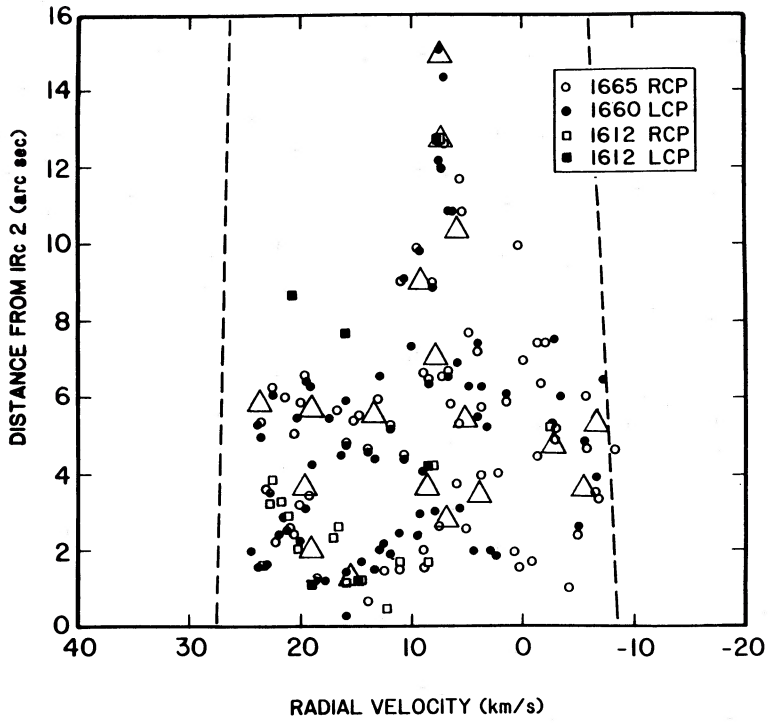

FIG. 6.—Outflow model for all OH masers in OMC-1. The distance of maser features from IRc2 vs. their radial velocity are plotted. The dotted lines show the bounds for an expanding sphere of radius 25″ and velocity 18 km s^{-1}, which is the model proposed by Genzel *et al.* (1981) for the low-velocity H_2O masers. The circles are the individual masers, while the triangles are the maser "clumps" listed in Table 3. A simple expanding sphere does not appear to fit the data.

posed by Plambeck *et al.* (1982), in which the S0 emission arises from an expanding "doughnut" of gas centered near IRc2. If there is an ambient cloud that is distributed along a NE and SW line, then a symmetric outflow of velocity ~15 km s^{-1} could produce the observed OH maser emission. This, also, would give rise to the appearance of a "doughnut" of gas where the H_2O masers are near the outer edge of the "doughnut," where the outflow has created the densest regions while the OH masers are found closer to the center of the outflow. The axis of the "doughnut" is along the line joining IRc2 and IRc6. The exciting source, therefore, will be along this line. Alternatively there could be two outflows, one near IRc2 and another near IRc6. The H_2 emission which is along the NW–SE directions is caused by an outflow into a region of lesser density than that defined by the "doughnut." This is consistent with maser emission near turbulent regions near the edges of shock fronts. Therefore, from the OH data one cannot distinguish between models which consist of a cavity or that of a complex outflow.

The magnetic field associated with OMC-1 can be estimated by studying the 1665 and the 1612 MHz spectra, if it is assumed that features approximately coincident in position between the RCP and LCP spectra have been split in velocity by the presence of a magnetic field (Hansen 1980). Table 4 lists the possible Zeeman pairs, which were identified by their positional coincidence, and their magnetic field strength. The magnetic field estimates are in the range 1–3 mG. The features with velocities between 5.6 km s^{-1} and 8.6 km s^{-1} agree with the Zeeman interpretation and calculations of Hansen *et al.* (1977), Hansen and Johnston (1983), and Norris (1984).

IV. CONCLUSIONS

The OH maser emission associated with Orion-KL has been mapped completely in the 1612 and 1665 MHz transitions to a flux density level of 0.5 Jy in the velocity range −5 to +25 km s^{-1}. The emission has been found to lie over a linear east-west distribution of 14″ in length encompassing the IR sources IRc2, IRc6, and IRc7 and is located along a ridge defined by the NH_3 hyperfine satellite "hot core" and plateau lines. Other areas of emission which are close to 8 km s^{-1} are found 5″–10″ from this emission. The OH emission appears to be in "clumps" with velocity dispersions of 2–6 km s^{-1}. The distribution of this emission appears to be quite complex and is not associated with a simple expansion from IRc2. The origin and distribu-

TABLE 4

ZEEMAN PAIRS

RCP		LCP		STRENGTH OF MAGNETIC FIELD (mG)
Velocity (km s^{-1})	Flux (Jy)	Velocity (km s^{-1})	Flux (Jy)	
1665 MHz				
23.4	0.7	23.9	0.4	2.1
5.6	1.6	6.4	3.2	3.2
1612 MHz				
14.6	2.1	14.9	0.4	1.1
8.1	7.8	8.6	4.3	1.8
7.5	1.2	7.8	0.7	1.4

tion of this emission seems to be in high density and temperature condensations which are probably found in turbulent areas near the edges of shock fronts. The OH emission is not inconsistent with a large irregular cavity surrounding IRc2 with the emission found in high density and temperature condensations on the edges of this cavity or that of an outflow plowing into a dense medium that is distributed along a NW–SE line. Alternatively, the OH masers could be near the central exciting source or sources giving rise to a cavity near the center of an outflow.

In order to determine accurate proper motions for the OH masers, further monitoring is necessary at more frequent intervals in order to improve the accuracy of the absolute and relative positions of both low-velocity and high-velocity features which may be associated with an outflow. Our data suggest that it is difficult to observe the same maser features in periods of over 4 yr, due to the variability found in the spectra. Therefore the positional accuracy of these measurements must be at the level of 0.5 mas to detect proper motions of a few km s^{-1}.

REFERENCES

Buhl, D., Snyder, L. E., Lovas, F., and Johnson, D. R. 1974, *Ap. J. (Letters)*, **192**, L97.
Genzel, R., Downes, D., Ho, P. T. P., and Bieging, J. H. 1982, *Ap. J. (Letters)*, **259**, L103.
Genzel, R., Reid, M. J., Moran, J. M., and Downes, D. 1981, *Ap. J.*, **244**, 884.
Hansen, S. S. 1980, Ph.D. thesis, University of Massachusetts.
———. 1982, *Ap. J.*, **260**, 599.
Hansen, S. S., and Johnston, K. J. 1983, *Ap. J.*, **267**, 625.
Hansen, S. S., Moran, J. M., Reid, M. J., Johnston, K. J., Spencer, J. H., and Walker, R. C. 1977, *Ap. J.*, **218**, 165.
Johnston, K. J., de Vegt, C., Florkowski, D. R., and Wade, C. M. 1985, *A.J.*, **90**, 2390.
Knowles, S. H., *et al.* 1969, *Science*, **163**, 1055.
Madalena, R. 1986, private communication.
Menon, T. K. 1967, *Ap. J. (Letters)*, **150**, L167.
Norris, R. P. 1984, *M.N.R.A.S.*, **207**, 127.
Norris, R. P., and Booth, R. S. 1981, *M.N.R.A.S.*, **195**, 213.
Palmer, P., and Zuckerman, B. 1967, *Ap. J.*, **148**, 727.
Pauls, T. A., Wilson, T. L., Bieging, J. H., and Martin, R. N. 1983, *Astr. Ap.*, **124**, 23.
Plambeck, R. L., Wright, M. C. H., Welch, W. J., Bieging, J. H., Baud, B., Ho, P. T. P., and Vogel, S. N. 1982, *Ap. J.*, **259**, 617.
Sullivan, W. T. 1973, *Ap. J.*, **222**, 393.
Wynn-Williams, C. B., Genzel, R., Becklin, E. E., and Downes, D. 1984, *Ap. J.*, **281**, 172.

K. J. JOHNSTON: Code 4130, Naval Research Laboratory, Washington, DC 20375-5000

V. MIGENES: University of Pennsylvania, Department of Astronomy and Astrophysics (E1), Philadelphia, PA 19104

R. P. NORRIS: CSIRO, Division of Radiophysics, P.O. Box 76, Epping, NSW, Australia 2121